ShortcutFusion: From Tensorflow to FPGA-based accelerator with reuse-aware memory allocation for shortcut data

Duy Thanh Nguyen, Hyeonseung Je, Tuan Nghia Nguyen, Soojung Ryu, Kyujung Lee, and Hyuk-Jae Lee, *Member*, *IEEE*

Abstract-Residual block is a very common component in recent state-of-the art CNNs such as EfficientNet/EfficientDet. Shortcut data accounts for nearly 40% of feature-maps access in ResNet152 [8]. Most of the previous DNN compilers/accelerators ignore the shortcut data optimization. This paper presents ShortcutFusion, an optimization tool for FPGA-based accelerator with a reuse-aware static memory allocation for shortcut data, to maximize on-chip data reuse given resource constraints. From TensorFlow DNN models, the proposed design generates instruction sets for a group of nodes which uses an optimized data reuse for each residual block. The accelerator design implemented on the Xilinx KCU1500 FPGA card significantly outperforms NVIDIA RTX 2080 Ti, Titan Xp, and GTX 1080 Ti for the EfficientNet inference. Compared to RTX 2080 Ti, the proposed design is 1.35-2.33× faster and 6.7-7.9× more power efficient. Compared to the result from baseline, in which the weights/inputs/outputs are accessed from the off-chip memory exactly once per each layer, ShortcutFusion reduces the DRAM access by 47.8-84.8% for RetinaNet, Yolov3, ResNet152, and EfficientNet. Given a similar buffer size to ShortcutMining [8], which also "mine" the shortcut data in hardware, the proposed work reduces off-chip access for feature-maps 5.27× while accessing weight from off-chip memory exactly once.

Index Terms— End-to-end, CNN accelerator, FPGA, shortcut reuse, reuse-aware, shared MAC

I. INTRODUCTION

THERE have been many works trying to reduce the complexity and model size of CNNs using depthwise convolution [1]-[5], [40]. However, the question whether they are really efficient when running on general-purpose processor, such as CPUs/GPUs, has not been studied thoroughly. A previous study [47] showed that depthwise convolution achieves low performance on both the training and inference of various deep learning frameworks such as Tensorflow [29], Darknet [24], and Pytorch [30].

- D. T. Nguyen, H.-S. Jae were with Department of Electrical and Computer Engineering, Seoul National University, Seoul 08826, Korea. They are now with Samsung Electronics, Korea (email: thanhnd@capps.snu.ac.kr)
- T. N. Nguyen, and H.-J. Lee are with the Inter-University Semiconductor Research Center, Department of Electrical and Computer Engineering, Seoul National University, Seoul 08826, Korea
- S.-J Ryu is with SK Telecom, Korea.
- K.-J. Lee is with the Department of Electronic Engineering, Sun Moon University, Asan, Korea

Corresponding authors: H.-J. Lee, K.-J. Lee.

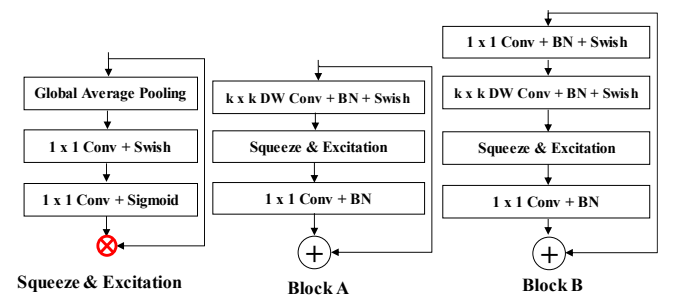


Fig. 1. Residual block with Squeeze & Excitation Optimization in EfficientNet/EfficientDet/MobileNet v3.

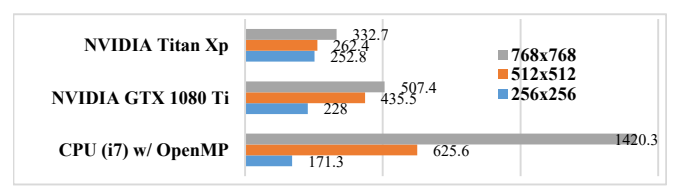


Fig. 2: Latency (ms) of the EfficientNet-B1 inference (batch size 1) for different input sizes.

Recent state-of-the-art compact CNNs such as EfficientNet [1], EfficientDet [2] and MobileNet v3 [40], which combine mobile inverted bottleneck (MBconv) [4] and Squeeze-and-Excitation optimization (SE block) [6] as shown in Fig. 1, have achieved a new record for high accuracy classification/detection/segmentation tasks while being less complex (i.e., BFLOPS) and more compact compared to previous works. For instance, EfficientNet-B1 achieved a higher accuracy than that of ResNet152 [22] (78.8 vs 77.8) with 7.6 times less parameters and 16 times less FLOPS. Despite being much more compact, its inference speed on an Intel CPU, NVIDIA Titan Xp (12 TFLOPS) and NVIDIA GTX 1080 Ti (11.3 TFLOPS) is not really fast shown in Fig. 2. For running on an edge accelerator such as the Google edge-TPU, the original EfficientNets are optimized by replacing depth-wise convolutions by normal convolutions and removing SE blocks at the cost of some accuracy loss [41]. Due to the very deep architecture and lightweight model, beside the kernel scheduling overhead, memory bottle-neck is also important factor to the inference of compact CNNs. For example, for a 768x768 input size and 8-bit precision, EfficientNet-B1 requires 13.34 BFLOPS and 475 MB of intermediate data access when the inputs/outputs are accessed from the off-chip memory exactly once while the model size is merely 9 MB.

There are previous works on end-to-end frameworks for accelerator designs on FPGAs [15]-[19], [33], [42]-[46]. FP-

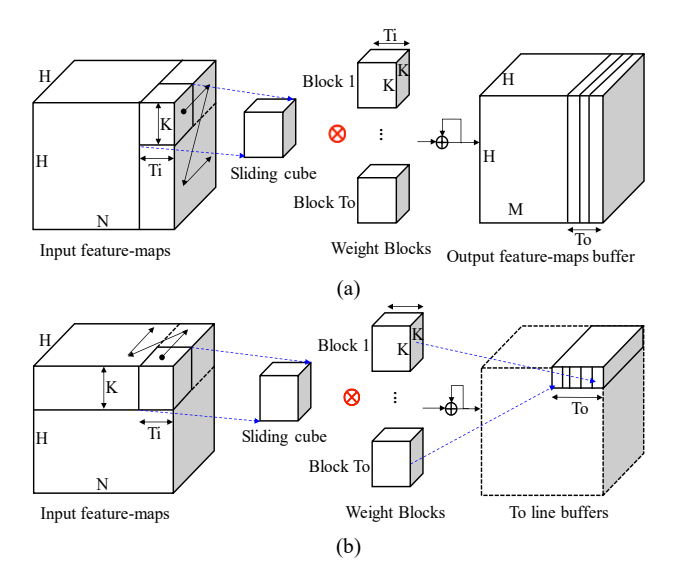


Fig. 3. The scheduling for streaming convolutional layer: (a) Frame-based weight reuse. (b) Row-based weight reuse. Borrowed from Fig. 2 in [23].

DNN in [15] allocates a minimal number of physical buffers in DRAM (not SRAM) as a memory pool for implementation; it does not leverage the on-chip buffer in the FPGA efficiently to reduce the off-chip access. Argus in [16] provides an end-toend framework for a multi-CLP type accelerator [53]. The studies in [18] and [19] also provide an end-to-end framework for a multi-layer processor. Because the BRAMs of a FPGA are not enough for multiple hardware units, the data have to be stored in the off-chip memory. Therefore, in [16], [18], and [19], a large amount of data access is required for deeper networks. Even though they work fine for shallow networks, their scalability to a wide range of CNNs is limited. There are existing frameworks from Tensorflow to FPGAs, such as in [17], [33], [42] and [44]-[46]. DNNWeaver [42] does not support layer fusion while the others only support the fusion of Convolution, Activation and Batch Norm and/or Pooling. As mentioned in [8], the shortcut connection accounts for 40% of the feature-maps access in Resnet-152. All of these frameworks do not support in-hardware flexible data reuse schemes and neglect cross-layer shortcut data optimization which might cause sub-optimal off-chip access.

There have been many previous studies on the dataflow of CNN computing [8]-[12], [51]. Among [9], FlexFlow [11], [12], and [51] which optimize the dataflow for a shallow network VGG16, SmartShuttle [12] achieves the highest number of MAC/DRAM accesses. It proposes to switch between two data reuse schemes: partial sum oriented and weight oriented. It requires 434.8 MAC/DRAM accesses (i.e., 214 MB) for running the CONV layers of VGG16. For a deeper network such as ResNet-152 or EfficientNet, larger off-chip accesses might cause a long latency because it requires larger data for shortcut connection and feature-maps. As reported in the paper, the buffer size, which is larger than 512 KB, does not help to reduce the DRAM access despite supporting flexible tiling factors. An efficient scheme needs to read the weights and feature-maps exactly once from the off-chip memory with a limited on-chip buffer.

The contributions of this paper are listed below.

- An end-to-end design flow from Tensorflow frozen model to CNN inference on an FPGA-based accelerator. A CNN compiler with reuse-aware static memory allocation which supports cross-layer shortcut reuse to overcome the challenge of latency optimization with on/off-chip memory constraints for a wide range of CNNs.
- A hardware accelerator architecture with shared MAC (Multiplication-and-ACcumulation) arrays that tailors the CNN compiler is presented.
- Comprehensive experiments demonstrate that ShortcutFusion is more efficient in reducing the off-chip access with a similar buffer size compared to the previous works. Even though ShortcutFusion is validated with FPGA-based accelerator in this study, ShortcutFusion is also applicable to ASIC design with a unified buffer to optimize both on-chip buffer size and off-chip DRAM access. It outperforms the recent CPUs/GPUs when running recent state-of-the-art SE-based **CNNs** such EfficientNet/EfficientDet/MobileNet v3.

II. BACKGROUND

Low latency with small batch size is very important in real time CNN inference. Therefore, this work optimizes the latency with batch size of 1. There are only two main weight block reuse schemes for the tiled-based convolutional computation: frame-based weight reuse and row-based weight reuse [23]. It should be noted that the weight reuse term here refers to each tiled weight block. For example, for a 3×3 CONV layer, each tiled weight block is $3\times3\times T_i\times T_o$, where T_i and T_o are the parallelism factors for input and output channels, respectively.

The computation of the row-based weight reuse scheme is depicted in Fig. 3(a). It should be noted that the inputs are loaded once in a row-by-row manner. The input sliding cube, while slides along the width of the input image, is convolved with T_o weight blocks each time to produce T_o temporary output values. These weight blocks are reused for a row. The input sliding cube then shifts T_i channels toward the end of N-input channels until all input channels are read. To finish the processing for one row, the entire weight of the model is accessed from the memory. Therefore, to process the whole input feature-maps, the weights are read H times.

Fig. 3(b) illustrates the computation flow of the frame-based weight reuse scheme. Because each weight block is reused for an entire frame (i.e., width × height), it needs to be read from the buffer exactly once. Therefore, only a small weight block needs to be buffered. It is noteworthy that the input/output feature-maps are accessed multiple times from the on-chip buffer. This scheme is efficient for layers with a large weight size and a small feature-map size, in which the input/output feature-maps can be accessed on-chip. Meanwhile, the latency of reading the weight blocks from the off-chip memory can be hidden by the computation of the sub-frame input.

III. SHORTCUTFUSION

A. Overview

A block diagram of the proposed framework is shown in Fig. 4. There have been many open-source deep learning

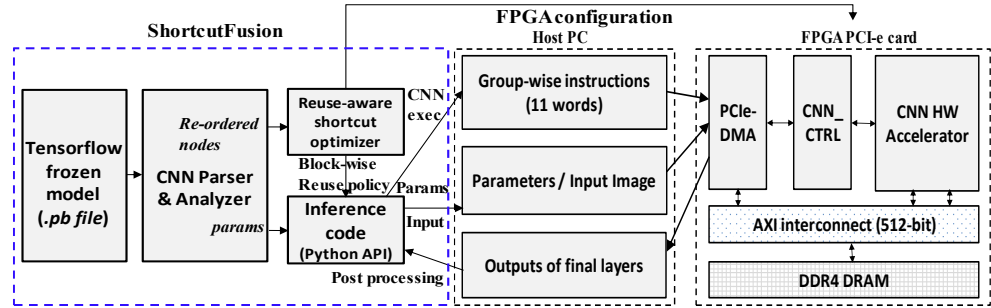


Fig. 4. Block diagram of the entire framework with ShortcutFusion.



(a) EfficientNet: CNN analyzer re-organizes 418 nodes to 139 groups for execution (b) Group-wise instructions Fig. 5. (a) Example of the CNN parser & analyzer for the EfficientNet protobuf file. (b) Instruction generation for off-loading the CNN to the FPGA.

frameworks for deep learning research: Tensorflow [29], Pytorch [30], Caffe [31] and Darknet [24]. Tensorflow is one of the most popular DNN frameworks that was developed by Google. Hence, this paper uses Tensorflow in the front-end of ShortcutFusion.

It is well known that a CNN is tolerant to errors. Previous research in [26] and [27] shows that 8-bit is efficient for various DNN inference tasks. The Google TPU [28] also uses 8-bit for both training and inference. Therefore, this study adapted an 8bit quantization for the accelerator design. The Tensorflow model file (protobuf file) is exported to the CNN parser & analyzer for parsing the architecture of the given CNN and extracting the quantized parameters. As depicted in Fig. 5 (a), the searched nodes of the CNN architecture are then reorganized into groups as supported by the back-end accelerator. Existing frameworks such as CloudDNN [17], [33], TensorRT [39] and Xilinx ML-Suite [44] support the fusion of CONV, Relu and BatchNorm and/or Pooling only. The lack of reuse of cross-layer shortcut data might cause large off-chip accesses thereby affecting the system performance. To address this issue, ShortcutFusion try to group as many nodes as possible to reduce the intermediate data movement and runtime overhead. example, Convolution, Activation, Normalization, Pooling, Element-wise (shortcut pass), and/or Up-sampling layers are fused together as supported in the backend accelerator. Like TensorRT, the feature-merging for concatenation in the row-reuse mode of this work also supports redirecting the output to the eventual destination of the concatenation to avoid data movement. The parameters extracted from the CNN parser & analyzer are used in the unified software reference code for hardware verification. In addition, the CNN architecture information is used in the Blockwise optimizer to select the optimal data access scheduling for each group of nodes in terms of the latency, on-chip buffer

requirement and DRAM access. The on-chip buffer selection and parallelisms are taken to configure the accelerator. It is noteworthy that the reuse-aware shortcut optimizer satisfies a strict constraint of the DRAM access, in which the parameters are accessed exactly once, the inputs/outputs of some layers are accessed from the DRAM exactly once, and the inputs/outputs of other layers are stored on-chip. This constraint is used in optimization problem in section IV-B (equation 10). Finally, the *inference code* generates instructions for entire layers of the CNN. As depicted in Fig. 5(b), the instruction sets of each node group consists of 11 words describing convolution size, activation type, pooling/upsampling option, fused elementwise, etc. It is noteworthy that the inference code packs parameters, input and all instructions and sends them at once to the hardware accelerator. The detail of the reuse-ware shortcut optimizer will be presented in section IV.

B. Architecture of the FPGA-based CNN accelerator to support ShortcutFusion

Fig. 6 describes the architecture of the accelerator that tailors ShortcutFusion. As mentioned in [8], the shortcut connection accounts for 40% of the feature-maps access in Resnet-152. Therefore, to maximize the shortcut data reuse, the proposed accelerator has an additional buffer for shortcut data. These physical buffers {0,1,2} are three interchangeable buffers for storing the input, output, shortcut data, or parameters of the entire layer. The group-wise dataflow controller is able to switch between two levels of weight reuse based on the pergroup instructions to balance between computation and off-chip memory access. The wide circular *row buffer* and double weight buffer provide the high bandwidth for feeding the sliding windows and weight to the parallel convolution kernels. The partial sum from the MAC arrays are stored temporarily in the *out buffer*. As different CNN layers may require different

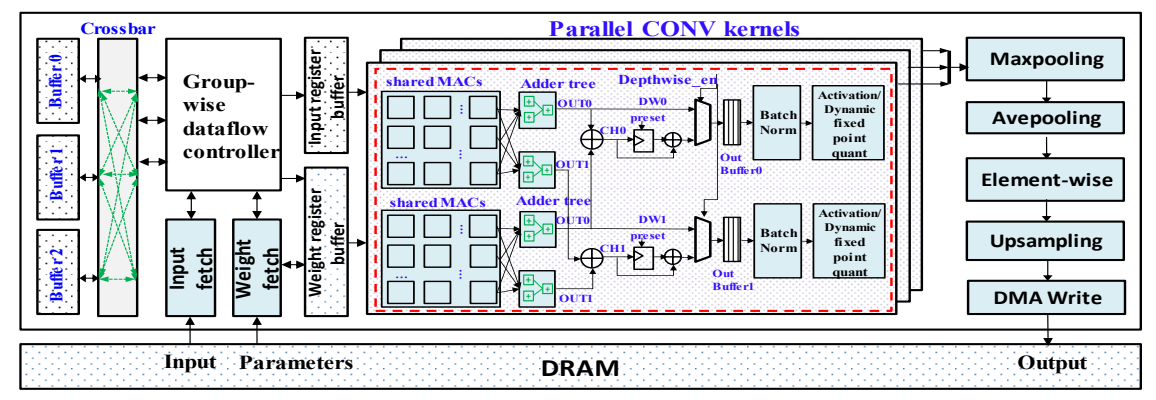
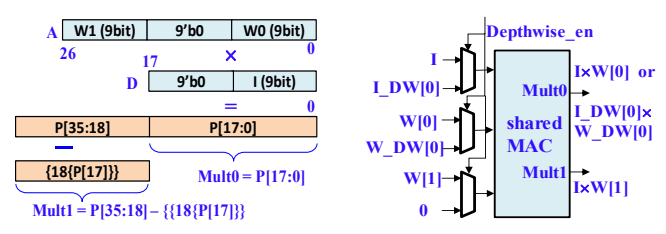


Fig. 6. Block diagram of the CNN accelerator.



(a) 2 signed 9×9 MULTs/DSP48E2. (b) a shared MAC.

Fig. 7. (a). Mapping of 2 signed 9x9 MULTs to a DSP48E2. (b). Shared MAC for a normal/depth-wise convolution.

value ranges for data, the proposed design supports a dynamic fixed point format to preserve the accuracy. Finally, there is a chain of modules such as max-pooling, average-pooling, element-wise addition, and up-sampling. The outputs from the parallel kernels are forwarded directly to this chain without storing back to the memory to reduce the data movement. It should be noted that these modules also support different data reuse schemes same as the convolutional module, thereby, have connection to the three physical buffers.

1) Convolution kernel design with shared MACs

A single DSP48E2 in Ultrascale and Ultrascale+ supports two INT8 multiplications sharing a same operand [32] to increase the DSP efficiency. As the proposed CNN accelerator targets multiple CNNs in various applications, it supports both 8-bit signed and unsigned feature-maps. In addition, the weights use 8-bit non-zero quantization which has been proved to have a higher accuracy compared to the zero-centered quantization [23]. Therefore, the proposed design requires signed 9x9 multiplication which is not inherently supported by DSP48E2 in the double MAC mode. To make it possible, a correction logic is added as described in Fig. 7(a), where $Mult0 = I \times W_0$, $Mult1 = I \times W_1$.

Double multiplication can be applied to the normal convolution because the input feature-maps are shared among the different weight filters. However, the depth-wise convolution does not have such input reuse. Fig. 7(b) shows the block design of a shared MAC. It supports double multiplications for the normal convolution and single multiplication for the depth-wise convolution. Finally, as depicted in Fig. 8, this study proposes a convolution kernel design with a *shared MAC array* to utilize the DSPs better. Fig. 8(a) depicts the mapping of a 3×3 depth-wise kernel to the

MAC array. Because the recent popular CNNs such as MobileNet v3, EfficientNet and EfficientDet use $1\times1/3\times3/5\times5$ depth-wise kernels, the MAC array is able to process a kernel in one cycle. In the case where the kernel size is greater than 7×7 , it needs multiple cycles for kernel processing. Fig. 8(b) shows the detailed mapping of two output kernels computation to the two MAC arrays. Sixty-four multiplications for each normal CONV kernel are interleaved into two *shared MAC* arrays, $I[63:0] \times W_{\{0:1\}}[63:0]$, whereas each depth-wise kernel is processed by separated MAC arrays: $I_DW_0[31:0] \times W_DW_0[31:0]$ (top array), $I_DW_1[31:0] \times W_DW_1[31:0]$ (bottom array). Depending on whether it is the normal or depth-wise CONV.

the output from the adder tree is forward to the accumulation unit or output buffer directly.

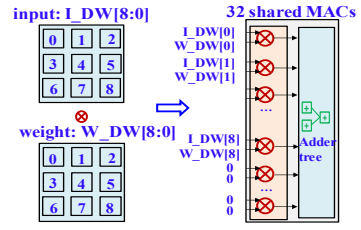
2) Shortcut data reuse in different weight reuse schemes

In order to realize ShortcutFusion, the back-end hardware need to support cross-layer shortcut data reuse. As illustrated in Fig. 9, the second inputs of the element-wise addition layer (shortcut layer) are fetched whenever the first inputs from the convolution kernels are available. Therefore, in the row-reuse mode, the fused layers (CONV+shortcut) require only one Write and two Reads instead of two Writes and three Reads from the off-chip memory. Similar to the row-reuse mode, the frame-reuse mode uses two less on-chip data movements. Moreover, the element-wise layer does not incur an additional timing overhead, thereby reducing the total latency.

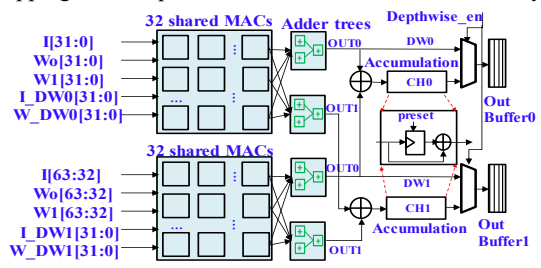
ShortcutMining [8] reuses shortcut data on-chip by reserving an untouched buffer space for shortcut data. Since it uses a fixed reuse scheme for all layers, it required a large buffer size. On the other hand, the proposed scheme carefully selects weight reuse scheme in the memory allocation for shortcut layer data, thereby very efficient in reducing both the total latency, off-chip access, and on-chip buffer size.

IV. REUSE-AWARE SHORTCUT OPTIMIZER

Because this study supports shortcut data reuse for different reuse schemes, the proposed scheme is able to switch the data reuse between blocks of CONV layers called block-wise data reuse. As shown in Fig. 10, a block of layers is defined as a residual block or a single CNN layer which does not belong to any residual blocks. Given the buffer constraints, the *proposed optimizer* searches for the optimal switching between two



(a) Mapping a 3x3 depthwise kernel to the shared MAC array



(b) Mapping of two normal/depthwise output kernels to 2 shared MAC arrays

Fig. 8. A kernel design with shared MACs for normal/depthwise convolutions.

weight reuse schemes (row-reuse and frame-reuse) for each block to get the optimized latency, on-chip buffer, and DRAM access. It should be noted that both the weights and featuremaps are read from the off-chip memory exactly once.

A cut-point is defined as the position in the CNN graph where the data reuse scheme switches. A CNN comprised of N basic blocks might have up to 2^N different switching schemes. The exhaustive search to find the optimum data reuse policy is impractical for general CNNs which have hundreds of layers. Moreover, given a buffer constraint, it is not possible to get an optimized reuse policy for all blocks because each block requires a different constraint for its distributed buffers. There is an observation that, in all the recent CNNs, the feature-map size monotonically increases or decrease in a certain sequence of blocks. Therefore, this study proposes a coarse-grained block-wise shortcut reuse scheme which has been validated by recent very deep CNNs. In the proposed relaxation, a sequence of increasing or decreasing size blocks is assumed to have exactly one cut-point. Cut-points divide a CNN into segments as illustrated in Fig. 11. Layers in a same segment uses the same weight reuse scheme. The number of cut-points depends on the CNN architecture varying from a plain structure or residual style to a multi-scale, multi-branch architecture. In Fig. 11, a classification CNN has a single cut-point because the CNN structure goes from the largest scale to the smallest scale. With the same intuition, an auto-encoder CNN has two cut-points. Fig. 12 shows the details of the CNN categorization according to the Feature Network which might require a different number of cut-points. Fig. 12(a) shows the object detector with the Feature Pyramid Network (FPN [34]). Yolov3 [21] and RetinaNet [36] also use an FPN network. These CNNs require two cut-points. PANet [35] fuses the feature-maps both topdown and bottom-up. Therefore, PANet requires three cutpoints. For the recent state-of-the-art detector/segmentation EfficientDet [2], the number of cutpoints depends on the number of BiFPN (Bidirectional Feature

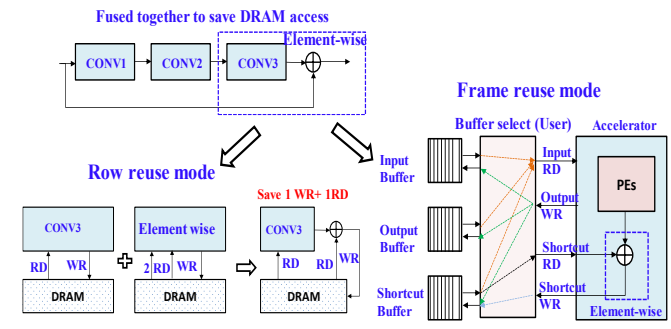


Fig. 9. Shortcut data reuse in row-reuse mode (left) and frame-reuse (right).

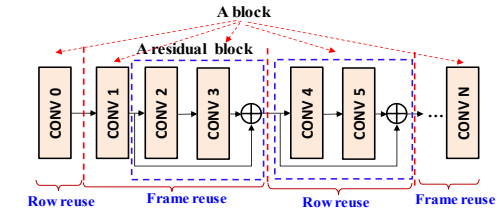


Fig. 10. Block-wise data reuse switching

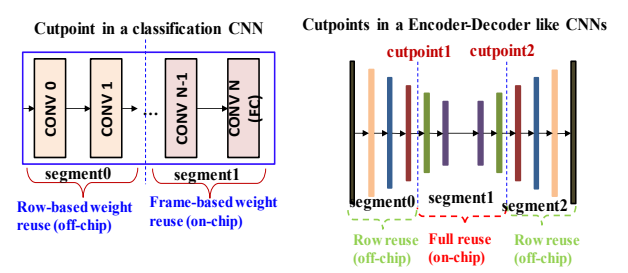


Fig. 11. Examples of a single cut-point (left) and double cut-points in CNNs.

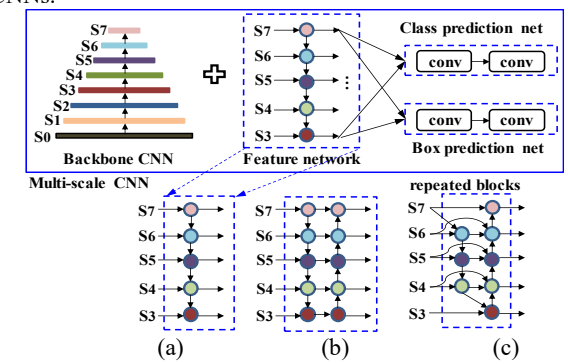


Fig. 12. Categorization of CNNs according to the architecture of the Feature Network. (a) FPN [34]. (b). PANet [35]. (c). BiFPN[2].

Pyramid Network) layers. For example, if the repeated block is one, there are only three cut-points because there are only one top-down and one bottom-up path aggregation. On the other hand, if there are more than one repeated block, the number of cut-points are equal to $(2 \times repeated_blocks+1)$.

The challenge is to find the cut-point positions to achieve the minimum latency while satisfying the buffer constraints and DRAM access constraints.

A. Reuse-aware static memory allocation

For the row-reuse mode, memory space for inputs, outputs and shortcuts are allocated in the off-chip memory. On the other hand, in the frame-reuse mode, the inputs, outputs and shortcuts are allocated to one of the three physical buffers to eliminate the off-chip access. Given the CNN architecture, the memory allocator statically allocates buffers for each layer by assigning three variables {alloc_input, alloc_output, alloc_shortcut} to {0, 1, 2} properly to reuse the shortcut data that is stored on-chip. It should be noted that the data of the long-path shortcut connection for concatenation is stored off-chip to avoid long lifetime data in the on-chip buffers.

Fig. 13 shows detailed examples of the on/off-chip memory access management for different network structures. In Fig. 13(a), networks with a plain structure such as VGGNet, Darknet19 and SimYolov2 [20] require only two buffers. On the other hand, the CNN with the residual block in Fig. 13(b) requires three buffers to reuse the shortcut data. The outputs from the last CONV layer in a residual block are forwarded to the Shortcut layer to reduce intermediate data access.

Fig. 13(c) and 13(d) shows the memory allocation for the residual block with the Squeeze-and-Excitation optimization with different weight reuse schemes. In the row-reuse mode as shown in Fig. 13(c), the outputs from Global Average Pooling and two FC layers are stored on-chip because their size is small. The last layer in the SE block is a scale layer (i.e., the red multiplier in the figure) that works in the same way as the 1x1 depthwise CONV layer without batch normalization. Different from the row-based reuse mode, the frame-reuse mode in Fig. 13(d) completely allocates data to three on-chip buffers. The outputs from the depthwise CONV layer (DW CONV) are stored in buffer B1. In parallel, the outputs from (DW CONV + Pooling) are stored in buffer B0 with an offset address to avoid overwriting the input in buffer B0. Similar to Fig. 13(c), the outputs from the two FC layers and data in buffer B1 serve as weights and inputs for the scale layer, respectively. The residual block with the SE optimization is known to be inefficient in GPUs even though it does not incur much computation overhead. This dataflow-aware static memory allocation and on-chip data forwarding are very efficient in reducing off-chip memory access for residual block with SE optimization.

B. Optimizing shortcut data reuse with given constraints

Let us denote that L is the data reuse policy. It is noteworthy that layers in a same basic block use the same data reuse. To calculate the required size for each buffer $\{0,1,2\}$ according to the data reuse L, the static buffer allocation for each layer i needs to be considered as shown at step 1 in Algorithm 1. $\{alloc_in(i), alloc_out(i), alloc_shortcut(i)\}$ are the buffer allocations for the input/output/shortcut data of layer i, respectively.

To derive the total raw SRAM size, the size of the following buffers need to be calculated: weight_buff, row_buff, out_buff, and write_buff. It is noteworthy that all the buffers have the same number of banks which are the parallelism factors T_i=T_o to remove the logic congestion of the buffer bank selection. In the row-reuse mode, the entire weights of a layer are pre-loaded to the on-chip buffer. Therefore, the required buffer size for a weight is as follows:

$$weight_buff(L) = max_{i=row\ reuse}weight_size(i)$$
 (1)

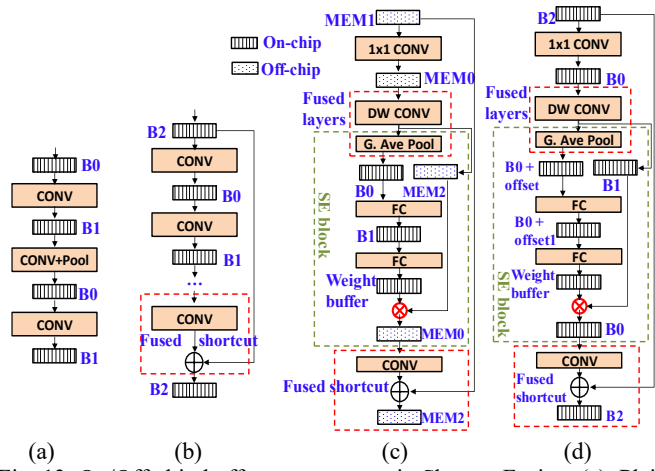


Fig. 13. On/Off-chip buffer management in ShortcutFusion. (a). Plain network. (b). Network with the residual block. (c) Residual block w/ the Squeeze-and-Excitation (SE) block in row-based weight reuse. (d). Residual block w/ the SE block in frame-based weight reuse.

It should be noted that the double weight block buffer for feeding weight blocks to parallel convolution kernels is stored in the LUT-RAMs of the FPGA chip because its depth is small $(2\times3\times3 = 18)$. Because buffer 1 is shared for both feature-maps and weights, the size of buffer 1 is as follows:

$$buff[1](L) = max(weight_buff(L), buff[1](L))$$
 (2)

The proposed convolutional kernel design focuses on the 3x3 normal convolution as in most of the CNNs and 1x1/3x3/5x5 depthwise convolutions for EfficientNet/Det. However, it can also support convolutions with a filter size larger than 7x7 by merely increasing the number of row buffers and double weight block buffer depth. Therefore, in the proposed design, there are six rows in the row buffer including one row for input prefetching:

$$row_buff(L) = max_i 6 \times in_rowsize(i) = max_i 6 \times w_i \times N_i$$
(3)

where w_i and N_i are the width and input channels, respectively. Regarding the buffer for temporarily partial sums, the buffer size for the frame-based reuse mode is larger than that for the row-based reuse mode because the row-reuse mode needs to buffer only one row. Therefore, the partial sum buffer (4-byte width) is derived as below:

$$out_buff(L) = max_{i=frame_reuse}out_{buff(i)}$$

= $max_{i=frame_reuse}out_w_i \times out_h_i \times T_o \times 4$ (4)

Finally, the output from the accelerator is buffered in the write buffer before writing to the off-chip memory. In the frame-based reuse mode, except for the final outputs of the CNN and long-path shortcut/concatenation, all intermediate data are stored on-chip. Therefore, the size of the write buffer is as below:

$$write_buff(L) = \max(\max_{i=row_reuse} write_buff(i), \\ \max_{i=frame_reuse\&i=final_layers} write_buff(i)) \\ = \max(\max_{i=row_reuse} out_w_i \times T_o, \\$$

Algorithm 1: Calculation of the required buffer size.

```
Input: CNN architecture with N layers
Output: required buffer size w.r.t. the data reuse
policy L: buff[0](L), buff[1](L), buff[2](L)
For each layer i in frame-reuse do
    {alloc in(i), alloc out(i), alloc shortcut(i)}
      = buff_alloc(layer i);
    buff[alloc in(i)](L) =
      max(buff[alloc_in(i)](L), input_size(i));
 3. if (to residual(i) == yes) // layer i is used for
residual layer
      buff[alloc shortcut(i)](L) =
 max(buff[alloc_shortcut(i)](L),output_size(i));
4. if (NextLayer(i) == Maxpool2x2) // fused conv+pool
      buff[alloc out(i)](L)
      max(buff[alloc out(i)](L), output size(i)/4);
    else
      buff[alloc out(i)](L) =
        max(buff[alloc out(i)](L), output size(i));
```

$$max_{i=frame_reuse\&i=final_layers} out_w_i \times out_h_i \times T_o) \ (5)$$

To sum them up, the required raw SRAM size is as follow:

$$\begin{split} SRAM size(L) &= row_buff(L) + out_buff(L) \\ + write_buff(L) + buff[0](L) + buff[1](L) + buff[2](L) \ (6) \end{split}$$

The raw SRAM size does not physically reflect the real BRAM utilization of a FPGA chip. Therefore, the number of BRAM 18k needed for each buffer is estimated as below:

$$BRAM18k = \left[\frac{buff_depth}{1024}\right] \left[\frac{buff_width}{18}\right] \tag{7}$$

Regarding the necessity of reducing the total DRAM access in a CNN computation, the previous study in [37] shows that the energy consumed by an off-chip access is much larger than that by an on-chip access or arithmetic operation in an ASIC chip. Therefore, it is important to constrain the off-chip access. The proposed design supports data forwarding as discussed in section III-B-2. Hence, the DRAM access for feature-maps, and total DRAM access are calculated as shown in (8), (9), respectively.

$$DRAM_FM(L) = \sum_{i=row_reuse, i=conv} (in_size(i) + out_size(i))$$

$$+ \sum_{i=row_reuse, i=shortcut} in_size(i)$$

$$+ \sum_{i=frame\ reuse, i=concat/route} 2 \times in_size(i)$$
 (8)

$$TotalDRAM(L) = DRAM_FM(L) + \sum_{i} weight_size(i)$$
 (9)

The optimization problem is to find the data reuse policy L as follows:

$$min_l(latency(L, T_i, T_o)) \text{ s.t.:}$$

$$DSP(T_i, T_o) < \alpha$$

$$BRAM18K(L, T_i, T_o) < \beta$$
(*)

weights access = 1, $feature\ maps\ access \le 1$ (10)

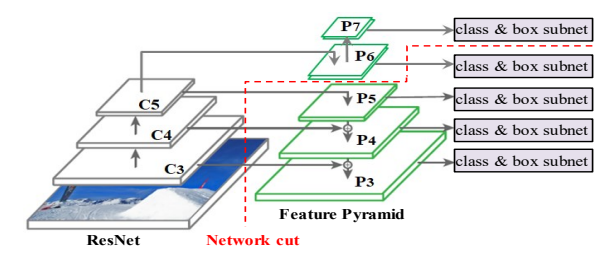


Fig. 14. RetinaNet with a network "cut."

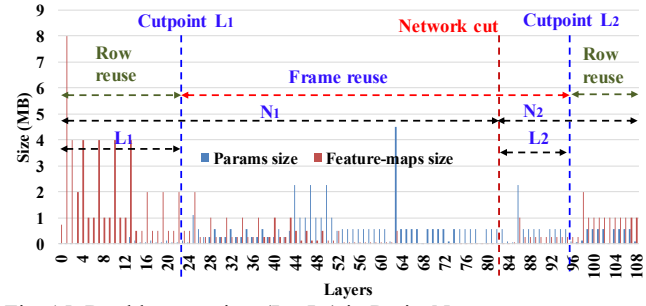


Fig. 15. Double cut-points (L1, L2) in RetinaNet.

where the constraint (10) is explained in section III-A.

A problem is raised such that the latency estimation by running the RTL simulation for each candidate takes a very long time. Because the number of candidates in the design space can be large, the RTL simulation approach is not feasible. Therefore, this work built a cycle-accurate timing simulator to estimate the latency of a CNN layer running different reuse schemes as described in Fig. 3 and Fig. 4. The latency estimation model was verified with the RTL simulation for the CNN with all the candidates for policy L in the design space. Single cut-point optimization: In Fig. 11 (left), the i-th layer is in the row-reuse mode if i < L and the frame-reuse mode, otherwise.

Multiple cut-points optimization: Fig. 14 shows an example of double cut-points in the RetinaNet. Network "cut" is the position that divides the RetinaNet into two sub-networks: from the beginning to the smallest scale and from the smallest scale to the end. From this network cut, the relative position of the data reuse policy L=(L_1 , L_2) is defined, as shown in Fig. 15, where $0 \le L_1 < N_1$, and $0 \le L_2 < N_2$. The real layer indexes of L are (L_1 , $N_1 + L_2$). Layer i=row_reuse if $i < L_1 \parallel i \ge N_1 + L_2$, and i=frame_reuse, otherwise. The other multiple cut-point cases can be extended with a same exhaustive search for the optimum policy in the polynomial of time $O(N^k)$, where N and k are the depth of the sub-networks and the number of the cut-points in the CNN, respectively.

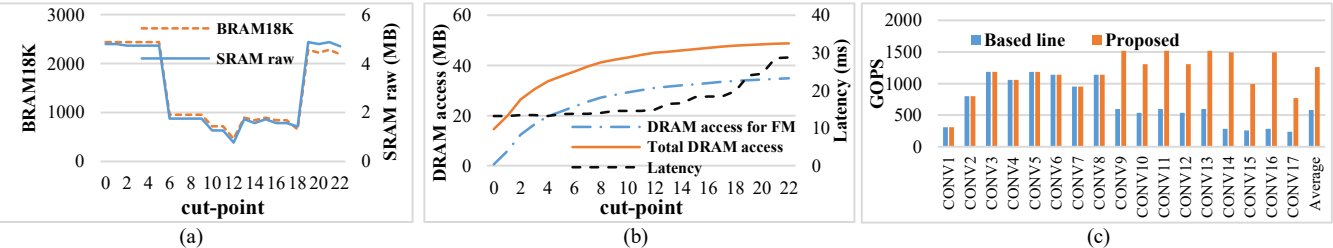


Fig. 16. Latency of the CONV layers in the YOLOv2 CNN with the fixed row-based reuse scheme and the coarse-grained reuse scheme.

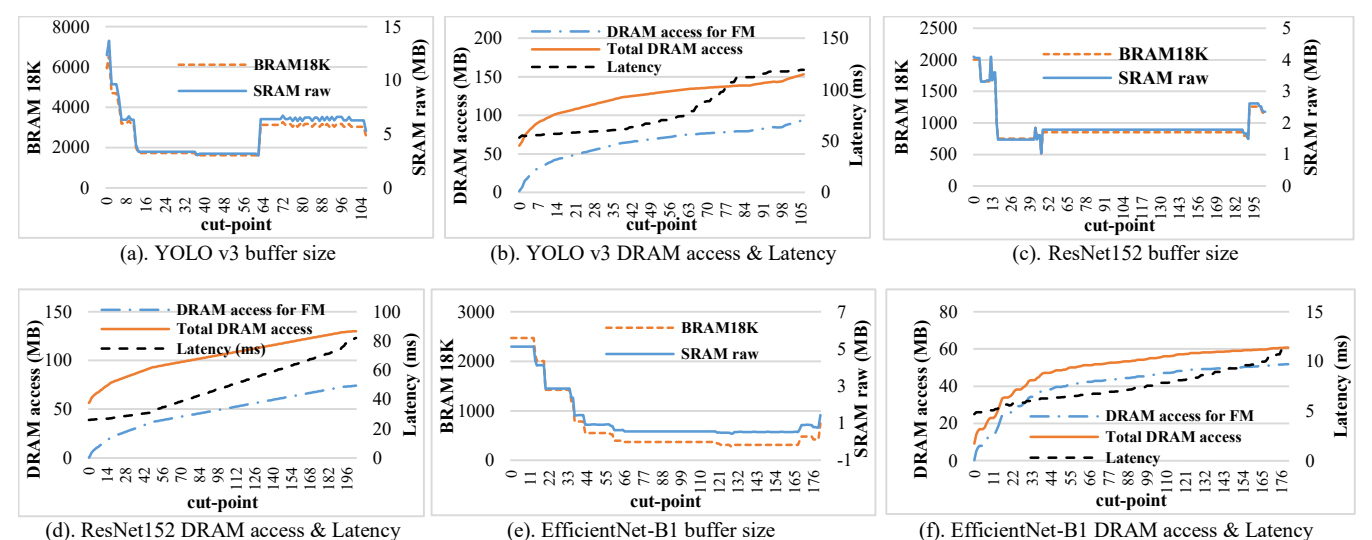


Fig. 17. The on/off chip access and latency w.r.t. the cut-point position for various CNNs: YOLO v3, ResNet152, and EfficientNet-B1.

TABLE I
RESNET152 - PERFORMANCE COMPARISON TO PREVIOUS WORKS

Features	HPCA'19 [8]	Proposed
FPGA board	VC707	KCU1500
Frequency	150 MHz	200 MHz
Logics (K)	283.8 (86%)	215.3 (33%)
DSPs	2800 (100%)	2240 (41%)
BRAM18K	2040 (99%)	1945 (45%)
Input size	224x224	224x224
Precision	16-bit	16-bit
Weights (MB)	112.6 MB	112.6 MB
Throughput	608.3 GOPS	607.5 GOPS
DSP efficiency	72.4%	71.1%
Weight Load	Multiple times	Once
Off-chip FMs	62.93 MB	11.97

V. EXPERIMENTAL RESULTS

A. Reuse-aware shortcut optimizer

Fig. 16(a), and 17(b) show the buffer size, DRAM access and latency (i.e., inference time per single image) with regard to the cut-point position for YOLO v2. The minimum SRAM required is 0.76 MB corresponding to layer 12 (CONV9). Compared to the *baseline* which uses a fixed row-based weight reuse scheme, the proposed scheme achieves a 2.17 times speed-up, as shown in Fig. 16(c), while requiring a 5.73 times smaller buffer size. The speed up is seen from CONV9 because the proposed scheme reuses feature-maps on-chip and the weight load time is hidden by frame-based computation (as shown in Fig. 4(a)).

Fig. 17 shows the performances of the various CNNs: YOLO v3 (77 CONV layers), ResNet152 (152 CONV layers), and EfficientNet-B1 (139 CONV layers) with respect to the switching point positions. The optimizer provides an exhaustive search to find the minimum buffer size that satisfies the DRAM access constraints. It should be noted that in Fig. 17, the weights are accessed exactly once. Hence, the total DRAM access is always larger than the DRAM access for the feature-maps (FM) by the amount of the weight size. It can be seen that for all CNNs, the cut-point at the beginning achieves a better latency at the cost of a larger buffer size. As long as the buffer constraints are satisfied, the frame-based weight reuse scheme

TABLE II MINIMUM BUFFER SIZE FOR EACH CNN

Networks	Input size	Number of layers[*]	Minimum required buffer size
YOLO v2	416x416	21	0.762 MB
VGG-CONV	224x224	13	0.712 MB
YOLO v3	416x416	106	1.682 MB
RetinaNet	512x512	137	2.392 MB
Resnet50/152	224x224	68/204	1.039 MB
EfficientNet-B1	256x256	181	0.43 MB

[*] including other layers such as shortcut, concatenation, etc.

TABLE III
BUFFER SIZE TO MINIMIZED OFF-CHIP ACCESS FOR VGG-CONV

-	OLAccel[38]	SmartShuttle[12]	Proposed	
Networks	VGG-CONV			
Precision	Mixed (4,8)	8-bit	8-bit	
SRAM size	2.4 MB	0.75 MB	0.712 MB	
DRAM access	42.8 MB	58.1 MB	42.8 MB	

is better than the row-based weight reuse scheme in terms of both latency and DRAM access reduction.

Table I presents the comparison of the proposed design over the previous work on the ResNet152 inference. For a fair comparison, the proposed accelerator is designed with 16-bit precision, and the BRAMs constraint is set similar to Shortcut Mining in [8]. In this case, each multiplication is mapped to a single DSP. The proposed scheme achieves a similar DSP efficiency while reducing the off-chip access for the weights and feature-maps significantly. Shortcut Mining uses a large number of parallel buffer banks which are shared for both the feature-maps and partial sums. Because the bit width of the partial sums is many fold larger than that of the feature-maps, some of the buffer space might be wasted. In addition to that, a fixed data reuse scheme in [8] might require a very high BRAM utilization and frequent off-chip access.

B. Minimum buffer size requirement to satisfy the DRAM access constraints

Table II shows the minimum required buffer size for various CNNs to meet the DRAM access constraints (equation 10). These buffer sizes are not only practical for small to medium

TABLE IV
PERFORMANCE OF THE VARIOUS CNNS USING THE PROPOSED SCHEME

	ResNet50	ResNet152	Yolo v2	YOLO v3	RetinaNet	EfficientNet-B1
Platform		Xilinx KCU1500				
Frequency			200	MHz		
Data format		8-bit				
Input size	256x256	256x256	416x416	416x416	512x512	256x256
CNN Size (GOP)	11.76	31.16	17.18	65.86	102.2	1.38
LUTs/FFs (K)	212.7/361.5	212.7/361.5	203.1/331.0	213.3/352.0	264.3/367.2	264.1/375.7
DSP utilization	2240	2240	2240	2240	2240	2240
BRAM18k	2368 (55%)	2368 (55%)	2304 (53%)	3020 (70%)	3766 (87%)	2594 (50%)
Latency (ms)	11.69	26.78	14.73	57.57	93.16	4.69
GOPS	1006	1163	1166	1142	1097	317.1
MAC Efficiency	61.4%	71.0%	71.2%	69.7%	67.0%	19.37%
Weight load	Once	Once	Once	Once	Once	Once
Off-chip FMs	0.19 MB	0.19 MB	0.66 MB	90.6 MB	136.4 MB	0.19 MB
Total off-chip [*]	59.09 MB	130.2 MB	48.9 MB	153.5 MB	261.34 MB	60.7 MB
Off-chip reduction	60.62%	56.7%	70.31%	60.34%	47.81%	84.81%

^[*] Total off-chip memory access if data (weights/inputs/outputs) are accessed exactly once.

 $\label{total variation} Table~V$ Comparison of End-To-End Frameworks On ResNet50 Inference

	ML-Suite	FPL'19	Cloud-	Proposed
	[44]	[33]	DNN [17]	-
Platform	VU9P	VU9P	VU9P	KCU1500
riatioriii	(16nm)	(16nm)	(16nm)	(20nm)
URAM size		270 Mb		
Frequency	500 MHz	125 MHz	214 MHz	200 MHz
Framework	Tensorflow	Tensorflow	Caffe	Tensorflow
Network		ResN	et50	
Input size	224x224	224x224	224x224	256x256
Precision	8-bit	8-bit	16-bit	8-bit
Latency	7.77ms	23.8ms	8.12ms	11.9ms
LUTs	612K	605K	696K	217K
DSPs	5493	6005	5489	2240
GOPS	1290	328	1235	1006
Data reuse	Fixed	Fixed	Fixed	Flexible
Shortcut reuse	No	No	No	Yes
& fusion in HW				
SRAM size	31.2 [*]	18.8 [*]	38.3 [*]	5.2
(MB)				
DSP	23.47%	21.85%	52.58%	56.14%
efficiency				

[*]: Ultra-RAM + BRAMs utilization

size FPGA chips but also ASIC chips where the size of the SRAM might dictate the chip size. For example, the Google TPU [28] consists of 28 MiB of on-chip buffer which accounts for 30% of the chip area. The DRAM access constraints limit the DRAM accesses which are also important to reduce the energy consumption for ASIC chips [37]. Table III compares the buffer size and DRAM access of the proposed scheme compared to previous works for the VGG16 CONV layers. With the same amount of DRAM access (i.e., input/output are accessed once), the proposed scheme requires a 3.4 times smaller buffer than [38] due to the adaptive reuse policy. Compared to SmartShuttle which proposes layer-wise data reuse schemes, the proposed scheme reduces DRAM access by 1.36 times with smaller on-chip buffer size. This demonstrates the efficiency of adaptive switching between row-based weight reuse schemes and frame-based weight reuse schemes over the reuse schemes using the tiled input/output in SmartShuttle.

Finally, the performance of various state-of-the-art CNNs using the proposed scheme are shown in Table IV. Depending on the on-chip buffer constraints, the proposed scheme

TABLE VI
EFFICIENTNET-B1 INFERENCE PERFORMANCE ON THE PROPOSED DESIGN

EFFICIENTINET-B1 INFERENCE PERFORMANCE ON THE PROPOSED DESIGN					
Resolution	256×256	512×512	768×768		
FPGA board	KCU1500				
Frequency	200 MHz				
LUTs/FFs (K)	264.1/375.7 264.5/375.5 271.7/375.4				
DSPs	2176				
BRAM18Ks	2594 (60%)	2723 (62%)	3845 (89%)		
GOPS	317.1	267.4	274.4		
DSP efficiency	19.37%	16.3%	16.75%		
Off-chip FMs	0.19 MB	144 MB	344 MB		
Total off-chip [*]	60.7 MB	216 MB	475 MB		
Off-chip Weights	Once				
Off-chip reduction	84.81%	29.2%	27.6%		
Power (W)	21.09	23.76	26.71		
GOPS/W	15.0	11.3	10.3		

[*]: Total off-chip memory access if weights/inputs/outputs are accessed from DRAM exactly once.

minimizes the DRAM access for the feature-maps while accessing parameters exactly once for all the CNNs due to strict off-chip access constraints in the proposed optimization. Compared to the baseline, in which all data are accessed off-chip exactly once, the proposed scheme reduces the total DRAM access by 47.8-84.8% for the various CNNs.

Table V shows the comparison of some end-to-end frameworks for the ResNet50 inference. All three previous works utilize large Ultra-RAM of a cloud-scale Xilinx FPGA which has 6840 DSPs and 270 Mb of Ultra-RAM. However, none of them support flexible data reuse. Whereas, the proposed framework supports adaptive data reuse schemes with inhardware shortcut fusion, thereby completely removing the off-chip access for intermediate data including the shortcut data while using less SRAM resource. Compared to Cloud-DNN, the proposed work utilizes 7.4× less SRAM resource while having 1.07× higher DSP efficiency. In addition, the proposed work achieves a competitive GOPS and 2.4× higher DSP efficiency than ML-Suite while requiring 6.0× less SRAM resource and running at 2.5× lower frequency.

C. Scalability and power efficiency for SOTA CNNs

A larger input size leads to higher accuracy while causing an increase in the on-chip buffer requirement, DRAM access and latency. Table VI presents the performance of the EfficientNet-

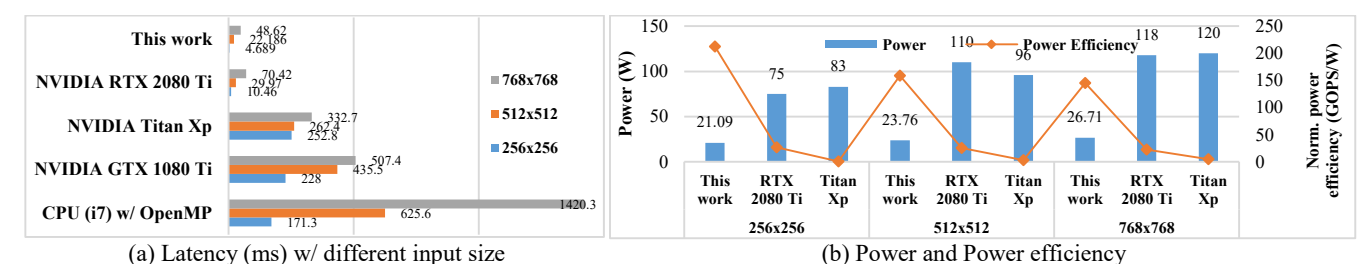


Fig. 18. Comparison of the proposed work and modern CPU/GPUs for EfficientNet-B1 inference (batch size = 1).

B1 inference with various high resolution images to demonstrate the scalability of the proposed scheme. For example, with a 768×768 input size, the total DRAM access if the inputs/outputs are accessed exactly once is 475 MB. Out of this, the proposed scheme requires only 344 MB for the feature-maps access which results in a 27.6% reduction. The reduction is 29.2% and 84.81% for 512×512 and 256×256, respectively.

The power of the accelerator is estimated as the sum of FPGA-chip power plus the DRAM power. The FPGA-chip power is calculated by Xilinx Power Estimator with the signal switching frequency from RTL simulation. The DRAM access energy is estimated from the total DRAM access and the energy per access from [56]. The CPU for experiment is Intel Xeon E3-1245 v5 3.5GHz with OpenMP enable. Meanwhile, GPU is tested with CUDA 10.0 and CuDNN. GPU power is calculated by nvidia-smi. Fig. 18 shows a detailed comparison of the proposed work with CPUs/GPUs. NVIDIA RTX 2080 Ti outperforms three other CPUs/GPUs in terms of both speed and power efficiency. In terms of speed, this work is 2.23, 1.35, and 1.45 times faster than NVIDIA 2080 Ti for 256×256, 512×512, and 768×768 input sizes, respectively. The reasons are the reduction of the DRAM access and more efficient hardware utilization for the residual block with SE optimization. In terms of power efficiency, this work is 6.3-7.9 times more power efficient than that of NVIDIA 2080 Ti. The DSP efficiency is low for EfficientNet (e.g., less than 20%) due to low density of multiplications in depthwise convolution. However, compared to GPUs, which has huge number of parallelism, the proposed design still shows significant speed up thanks to the reuseaware static memory allocation and shared MAC design.

VI. RELATED WORKS

Hardware accelerators use various dataflows to increase resource utilization, for example, weight stationary [7], [8], [16], [28], [48], [53], output stationary [49], and row stationary [13], [50], [51]. MAESTRO [52] analyzes the energy-performance trade-off for the various dataflows above to choose an optimized one for a given CNN. These fixed dataflow designs result in a sub-optimal on-chip buffer size and off-chip memory access when running different layers of a CNN with different characteristics. FlexFlow [11] presents an optimization from the on-chip buffer to the PEs enabling the mixing of multiple parallelism types of the feature-maps, neurons, and synapses to boost resource utilization which is orthogonal to the proposed work. DNA [10], and SmartShuttle [12] propose using a layer-wise data reuse scheme which supports switching between two of the three schemes: Input-Reuse, Output-Reuse and Weight-

Reuse. These works reduce the off-chip access efficiently compared to previous works which have a similar global buffer size. However, in these works, a larger buffer size (i.e., 512 KB) has less benefits even though the accelerator supports a flexible tile size.

In the literature, there are some compilers to schedule a FPGA-based CNN accelerator such as TVM [43], Xilinx ML-Suite [44], Intel DLA [45], and DNNVM [46]. TVM optimizes the standard CNN inference on the software side for a vanilla deep learning accelerator by overlapping the tensor computation with the memory load/store operations. However, the machine learning-based optimization for tuning each convolution layer has a considerable time cost which is burdensome for very deep networks. DLA optimizes CNN graph by adding a 1x1 identity layer and merging element-wise addition to the previous layer. Finally, ML-Suite and DNNVM fuse many adjacent layers such as convolution, batch norm, Relu, and pooling to reduce the off-chip access for intermediate data. Nevertheless, the lack of an in-hardware flexible data reuse and shortcut reuse reduces the MAC efficiency. Whereas, the proposed hardware/software co-optimizer, while being fast, provides adaptive data reuses to minimize the off-chip memory access and improve the MAC efficiency even with the on-chip buffer constraints.

VII. CONCLUSION

This paper presents a tool for FPGA-based CNN inference which uses a reuse-aware shortcut optimizer to minimize the latency, the off-chip memory access and improve the MAC efficiency given the on-chip buffer constraints. Comprehensive comparisons to previous works demonstrate the efficiency of the proposed approach. In addition, the proposed work achieves superior performance compared to NVIDIA GPUs when running state-of-the-art Squeeze-and-Excitation-based CNNs such as EfficientNets/EfficientDet/MobileNet v3.

REFERENCES

- M. Tan, Q. V. Le, "EfficientNet: Rethinking Model Scaling for Convolutional Neural Networks," [Online]. Available: arxiv.org/abs/1905.11946, 2020.
- [2] M. Tan, R. Pang, Q. V. Le, "EfficientDet: Scalable and Efficient Object Detection," [Online]. Available: arxiv.org/abs/1911.09070v7, 2020.
- [3] A. G. Howard, M. Zhu, B. Chen, D. Kalenichenko, W. Wang, T. Weyand, M. Andreetto, H. Adam, "MobileNets: Efficient Convolutional Neural Networks for Mobile Vision Applications," [Online]. Available: arxiv.org/abs/1704.04861, 2017.
- [4] M. Sandler, A. Howard, M. Zhu, A. Zhmoginov, L.-C. Chen, "MobileNetV2: Inverted Residuals and Linear Bottlenecks," in *Proc. IEEE Conf. Comput. Vis. Pattern Recognit.* (CVPR), 2018.

- [5] X. Zhang, X. Zhou, M. Lin, J. Sun, "ShuffleNet: An Extremely Efficient Convolutional Neural Network for Mobile Devices,"," in *Proc. IEEE Conf. Comput. Vis. Pattern Recognit. (CVPR)*, 2017.
- [6] J. Hu, L. Shen, G. Sun, "Squeeze-and-excitation networks," in *Proc. IEEE Conf. Comput. Vis. Pattern Recognit.* (CVPR), 2018.
- [7] M. Alwani, H. Chen, M. Ferdman, and P. Milder, "Fused-layer CNN accelerators," in *Proc. IEEE/ACM Int. Symp. Microarchitecture (MICRO)*, 2016.
- [8] A. Azizimazreah, L. Chen, "Shortcut Mining: Exploiting Cross-layer Shortcut reuse in DCNN Accelerator," in *Proc. IEEE Int. Symp. High Perf. Comput. Archit. (HPCA)*, 2019.
- [9] X. Chen, Y. Han, Y. Wang, "Communication lower bound in convolutional accelerator," in *Proc. IEEE Int. Symp. High Perf. Comput.* Archit. (HPCA), 2020.
- [10] F. Tu, S. Yin, P. Ouyang, S. Tang, L. Liu, S. Wei, "DNA: Deep Convolutional Neural Network Architecture with Reconfigurable Computation Patterns," in *IEEE Trans. Very Large Scale Integr. (VLSI)* Syst., vol. 25, no. 8, pp. 2220-2233, 2017.
- [11] W. Lu, G. Yan, J. Li, S. Gong, Y. Han, X. Li, "FlexFlow: A Flexible Dataflow Accelerator Architecture for Convolutional Neural Networks," in Proc. IEEE Int. Symp. High Perf. Comput. Archit. (HPCA), 2017.
- [12] J. Li, G. Yan, W. Lu, S. Jiang, S. Gong, J. Wu, X. Li, "SmartShuttle: Optimizing Off-Chip Memory Accesses for Deep Learning Accelerators," in *Proc. Des. Auto. & Test in Europe Conf. (DATE)*, 2018.
- [13] Y.-H. Chen, T.-J Yang, J. Emer, V. Sze, "Eyeriss v2: A Flexible Accelerator for Emerging Deep Neural Networks on Mobile Devices," in IEEE Journal of Emerg. Sel. Topics Circuits Syst. (JETCAS), vol. 9, no. 2, pp. 292-308, 2019.
- [14] L. Bai, Y. Zhao, X. Huang, "A CNN accelerator on FPGA using depthwise Separable Convolution," in IEEE Trans. Circuit Syst.-II: Express briefs, Vol. 65, No. 10, 2018.
- [15] Y. Guan, H. Lang, N. Xu, W. Wang, S. Shi, X. Chen, G. Sun, W. Zhang, J. Cong, "FP-DNN: An Automated Framework for Mapping Deep Neural Networks onto FPGAs with RTL-HLS Hybrid Templates," in *IEEE Annu. Int. Symp. Field-Programmable Custom Comput. Machine (FCCM)*, 2017.
- [16] Y. Shen, T. Ji, M. Ferdman, P. Milder, "Argus: An End-to-End Framework for Accelerating CNNs on FPGAs," in *Proc. IEEE/ACM Int. Symp. Microarchitecture (MICRO)*, 2019.
- [17] Y. Chen, J. He, X. Zhang, C. Hao, D. Chen, "Cloud-DNN: An Open Framework for Mapping DNN Models to Cloud FPGAs," in *Proc.* ACM/SIGDA Int. Symp. Field-Program. Gate Arrays (FPGA), 2019.
- [18] M. Blott, T. B. Preuber, N. J. Fraser, G. Gambardella, K. O'brien, Y. Omuroglu, M. Leeser, K. Vissers, "FINN-R: An End-to-End Deep-Learning Framework for Fast Exploration of Quantized Neural Networks," in ACM Trans. Reconfigurable Technol. Syst. (TRETS), vol. 11, no. 3, Artical 16, pp. 1-23, 2018.
- [19] X. Zhang, X. Zhang, J. Wang, C. Zhu, Y. Lin, J. Xiong, W. Hwu, D. Chen. "DNNBuilder: an Automated Tool for Building High-Performance DNN Hardware Accelerators for FPGAs," in Proc. Int. Conf. Comput-Aided. Des. (ICCAD), 2018.
- [20] J. Redmon, A. Farhadi, "YOLO9000: Better, Faster, Stronger," [Online]. Available: arxiv.org/abs/1612.08242.
- [21] J. Redmon, A. Farhadi, "YOLOv3: An Incremental Improvement," [Online]. Available: arxiv.org/abs/1804.02767.
- [22] K. He, X. Zhang, S. Ren, J. Sun, "Deep residual learning for image recognition", [Online]. Available: arxiv.org/abs/1512.03385.
- [23] D. T. Nguyen, T. N. Nguyen, H. Kim, and H.-J Lee. "A High-Throughput and Power-Efficient FPGA Implementation of YOLO CNN for Object Detection," in *IEEE Trans. Very Large Scale Integr. (VLSI) Syst.*, vol. 27, no. 8, pp. 1861-1873, 2019.
- [24] J. Redmon, "Darknet: An Open Source Neural Networks in C," 2013.
- [25] C. Zhang, P. Li, G. Sun, Y. Guan, B. Xiao, and J. Cong, "Optimizing FPGA-based accelerator design for deep convolutional neural networks," in *Proc. ACM/SIGDA Int. Symp. Field-Program. Gate Arrays (FPGA)*, 2015
- [26] S. Zhou, Y. Wu, Z. Ni, X. Zhou, H. Wen, and Y. Zou, "Dorefa-net: Training low bitwidth convolutional neural networks with low bitwidth gradients," [Online]. Available: arxiv.org/abs/1606.06160.

- [27] S. Han, H. Mao, and W. J. Dally, "Deep compression: Compressing deep neural networks with pruning, trained quantization and huffman coding," [Online]. Available: arxiv.org/abs/1510.00149.
- [28] N. P. Jouppi, C. Young, N. Patil, D. Patterson, G. Agrawal, R. Bajwa, S. Bates, S. Bhatia, N. Boden, A. Borchers, et al., "In datacenter performance analysis of a tensor processing unit," in *Proc. Int. Symp. Comput. Archit.(ISCA)*, 2017.
- [29] M. Abadi et al., TensorFlow: Large-scale machine learning on heterogeneous systems, 2015. Software available from tensorflow.org.
- [30] Paszke et al., PyTorch: An Imperative Style, High-Performance Deep Learning Library. Available: https://pytorch.org.
- [31] Y. Jia, E. Shelhamer, J. Donahue, S. Karayev, J. Long, "Caffe: Convolutional architecture for fast feature embedding", in *Proc. 22nd ACM Int. Conf. Multimed.*, 2014.
- [32] Ultrascale and Ultrascale+ FPGA, "Deep Learning with INT8 Optimization on Xilinx Devices," Xilinx, 2017.
- [33] S. Hadjis, K. Olukuntun, "Tensorflow to cloud FPGA: Tradeoffs for accelerating Deep Neural Networks," Proc. 22nd ACM Int. Conf. Multimed., 2019.
- [34] T.-Y. Lin, P. Doll'ar, R. Girshick, K. He, B. Hariharan, and S. Belongie, "Feature pyramid networks for object detection,"," in *Proc. IEEE Conf. Comput. Vis. Pattern Recognit. (CVPR)*, 2017.
- [35] S. Liu, L. Qi, H. Qin, J. Shi, and J. Jia, "Path aggregation network for instance segmentation,"," in Proc. IEEE Conf. Comput. Vis. Pattern Recognit. (CVPR), 2018.
- [36] T.-Y. Lin, P. Doll'ar, R. Girshick, K. He, B. Hariharan, and S. Belongie, "Focal loss for dense object detection," in *Proc. Int. Conf. Comput. Vis.* (ICCV), 2017.
- [37] S. Han, J. Pool, J. Tran, W. J. Dally, "Learning both weights and connections for efficient neural network,". [Online]. Available: arxiv.org/abs/1506.02626.
- [38] E. Park, D. Kim, S. Yoo, "Energy-efficient Neural Network Accelerator Based on Outlier-ware Low-precision Computation," in *Proc. Int. Symp. Comput. Archit. (ISCA)*, 2018.
- [39] TensorRT, June 2019. https://developer.nvidia.com/tensorrt.
- [40] A. Howard, M. Sandler, G. Chu, L.-C. Chen, B. Chen, M. Tan, W. Wang, Y. Zhu, R. Pang, V. Vasudevan, Quoc V. Le, H. Adam, "Searching for MobileNetV3," in *Proc. Int. Conf. Comput. Vis. (ICCV)*, 2019.
- [41] https://ai.googleblog.com/2019/08/efficientnet-edgetpu-creating.html.
- [42] H. Sharma, J. Park, D. Mahajan, E. Amaro, J. K. Kim, C. Shao, A. Mishra, H. Esmeilzadeh, "From high-level deep neural models to FPGAs," in Proc. IEEE/ACM Int. Symp. Microarchitecture (MICRO), 2016.
- [43] T. Chen, T. Moreau, Z. Jiang, L. Zheng, E. Yan, H. Shen, M. Cowan, L. Wang, Y. Hu, L. Ceze, C. Guestrin, and A. Krishnamurthy, "TVM: An automated end-to-end optimizing compiler for deep learning," in USENIX Symp. Operating Syst. Design and Implementation (OSDI), 2018.
- [44] Xilinx, "Xilinx DNN processor: An inference engine, network compiler and runtime for Xilinx FPGAs." in Hot Chips, 2018.
- [45] M. S. Abdelfattah, D. Han, A, Bitar, R. DiCecco, S. O'Connell, N. Shanker, J. Chu, I. Prins, J. Fender, A. C. Ling, G. R. Chiu, "DLA: Compiler and FPGA overlay for neural network inference acceleration," in *Proc. Int. Conf. Field Programmable Logic and Appl. (FPL)*, 2018.
- [46] Y. Xing, S. Liang, L. Sui, X. Jia, J. Qiu, X. Liu, Y. Wang, Y. Shan, and Y. Wang, "DNNVM: End-to-End Compiler Leveraging Heterogeneous Optimizations on FPGA-Based CNN Accelerators," in *IEEE Trans. Comput.-Aided Des. of Integr. Circuits Syst. (TCAD)*, 2020.
- [47] Z. Qin, Z. Zhang, D. Li, Y. Zhang, Y. Peng, "Diagonalwise Refactorization: An Efficient Training Method for Depthwise Convolutions," [Online]. Available: arxiv.org/pdf/1803.09926, 2018.
- [48] J. Qiu, J. Wang, S. Yao, K. Guo, B. Li, E. Zhou, J. Yu, T. Tang, N. Xu, S. Song et al., "Going deeper with embedded fpga platform for convolutional neural network," in *Proc. ACM/SIGDA Symp. Field-Program. Gate Arrays (FPGA)*, 2016.
- [49] Z. Du, R. Fasthuber, T. Chen, P. Ienne, L. Li, T. Luo, X. Feng, Y. Chen, and O. Temam, "Shidiannao: Shifting vision processing closer to the sensor," in *Proc. Int. Symp. Comput. Archit.(ISCA)*, 2015.
- [50] M. Gao, J. Pu, X. Yang, M. Horowitz, and C. Kozyrakis, "Tetris: Scalable and efficient neural network acceleration with 3d memory," in *Proc. Int. Conf. Archit. Support Program. Languages Operating Syst. (ASPLOS)*, 2017.

- [51] Y.-H. Chen, J. Emer, and V. Sze, "Eyeriss: A spatial architecture for energy-efficient dataflow for convolutional neural networks," in *Proc. Int.* Symp. Comput. Archit. (ISCA), 2016.
- [52] H. Kwon, P. Chatarasi, M. Pellauer, A. Parashar, V. Sarkar, and T. Krishna, "Understanding reuse, performance, and hardware cost of dnn dataflow: A data-centric approach," in *Proc. IEEE/ACM Int. Symp. Microarchitecture (MICRO)*, 2019.
- [53] Y. Shen, M. Ferdman, P. Milder, "Maximizing CNN Accelerator Efficiency Through resource partitioning," in *Proc. Int. Symp. Comput. Archit. (ISCA)*, 2017.
- [54] A. Parashar, P. Raina, Y. S. Shao, Y. Chen, V. A. Ying, A. Mukkara, R. Venkatesan, B. Khailany, S. W. Keckler, and J. Emer, "Timeloop: A systematic approach to dnn accelerator evaluation," in *Proc. IEEE Int. Symp. Perf. Anal. Syst. Softw. (ISPASS)*, March 2019.
- [55] X. Yang, M. Gao, Q. Liu, J. Setter, J. Pu, A. Nayak, S. Bell, K. Cao, H. Ha, P. Raina, C. Kozyrakis, and M. Horowitz, "Interstellar: Using Halide's Scheduling Language to Analyze DNN Accelerators," in *Proc. Int. Conf. Archit. Support Program. Languages Operating Syst.* (ASPLOS), Mar 2020.
- [56] K. T. Malladi, B. C. Lee, F. A. Nothaft, C. Kozyrakis, K. Periyathambi, and M. Horowitz, "Towards energy-proportional datacenter memory with mobile DRAM," in *Proc. Int. Symp. Comput. Archit. (ISCA)*, 2012.